Theoretical Studies To Understand Surface Chemistry on Carbon Anodes for Lithium-Ion Batteries: Reduction Mechanisms of Ethylene Carbonate

Yixuan Wang,*,† Shinichiro Nakamura,‡ Makoto Ue,‡ and Perla B. Balbuena*,†

Contribution from the Department of Chemical Engineering, Swearingen Engineering Center, University of South Carolina, Columbia, South Carolina 29208, and MCC-Group Science & Technology Research Center, Mitsubishi Chemical Corporation, Yokohama 227-8502, Japan

Received June 19, 2001

Abstract: Reductive decomposition mechanisms for ethylene carbonate (EC) molecule in electrolyte solutions for lithium-ion batteries are comprehensively investigated using density functional theory. In gas phase the reduction of EC is thermodynamically forbidden, whereas in bulk solvent it is likely to undergo one- as well as two-electron reduction processes. The presence of Li cation considerably stabilizes the EC reduction intermediates. The adiabatic electron affinities of the supermolecule $Li^+(EC)_n$ ($n = 1-4$) successively decrease with the number of EC molecules, independently of EC or Li^+ being reduced. Regarding the reductive decomposition mechanism, $Li^+(EC)_n$ is initially reduced to an ion-pair intermediate that will undergo homolytic C−O bond cleavage via an approximately 11.0 kcal/mol barrier, bringing up a radical anion coordinated with Li^+. Among the possible termination pathways of the radical anion, thermodynamically the most favorable is the formation of lithium butylene dicarbonate, $(CH_2CH_2OCO_2Li)_2$, followed by the formation of one O−Li bond compound containing an ester group, $LiO(CH_2)_2CO_2(CH_2)_2OCO_2Li$, then two very competitive reactions of the further reduction of the radical anion and the formation of lithium ethylene dicarbonate, $(CH_2OCO_2Li)_2$, and the least favorable is the formation of a C−Li bond compound (Li carbides), $Li(CH_2)_2OCO_2Li$. The products show a weak EC concentration dependence as has also been revealed for the reactions of $LiCO_3^-$ with $Li^+(EC)_n$; that is, the formation of Li_2CO_3 is slightly more favorable at low EC concentrations, whereas $(CH_2OCO_2Li)_2$ is favored at high EC concentrations. On the basis of the results presented here, in line with some experimental findings, we find that a two-electron reduction process indeed takes place by a stepwise path. Regarding the composition of the surface films resulting from solvent reduction, for which experiments usually indicate that $(CH_2OCO_2Li)_2$ is a dominant component, we conclude that they comprise two leading lithium alkyl bicarbonates, $(CH_2CH_2OCO_2Li)_2$ and $(CH_2OCO_2Li)_2$, together with $LiO(CH_2)_2CO_2(CH_2)_2OCO_2Li$, $Li(CH_2)_2OCO_2Li$ and Li_2CO_3.

Introduction

Lithium-ion batteries have been attracting much attention in the recent decades due to their very high energy density. A typical lithium-ion battery system is made up of a graphite anode, a nonaqueous organic electrolyte that acts as an ionic path between electrodes and separates the two materials, and a transition metal oxide (such as $LiMn_2O_4$, $LiNiO_2$) cathode. The most popular electrolytes are the mixtures of alkyl carbonates, for example, ethylene carbonate (EC) and propylene carbonate (PC), and lithium salts such as $LiClO_4$ and $LiPF_6$. It is commonly known that some organic electrolytes are decomposed during the first lithium intercalation into graphite to form a solid electrolyte interphase (SEI) film on the graphite anode surface, and it is the SEI film that largely determines the performance of graphite as anode in rechargeable batteries.[1] For instance, the higher the film-passivating ability, the better capacity and longer life cycle of the lithium-intercalated graphite anodes. Due to the high technological importance of this issue, extensive and intensive efforts are devoted to study the film-formation mechanism, as well as its structure and chemical composition using a wide variety of advanced techniques. Two different physical pictures are commonly adopted to explain the SEI film formation in carbonate-based electrolytes. Besenhard et al. suggested that the solvent can cointercalate into the graphite structure to form a ternary graphite intercalation compound (GIC) $[Li(sol)_yC_n]$, and its decomposition products determine the fate of the reaction behavior.[2,3] Another picture, originally proposed by Peled et al.[4,5] and further developed by Aurbach et al.,[6] postulates that the initial surface film controls the nature of further reactions. These two views mainly differ on whether the primary step of interface formation begins with GIC or with the electrochemical reduction of electrolyte on the surface.

† University of South Carolina.

‡ Mitsubishi Chemical Corporation.

(1) Dominey, L. A. *In Lithium Batteries: New Materials, Developments and Perspectives*; Elsevier: Amsterdam, New York, London, Tokyo, 1994.

(2) Besenhard, J. O.; Winter, M.; Yang, J.; Biberacher, W. *J. Power Sources* **1995**, *54*, 228.

(3) Winter, M.; Besenhard, J. O. In *In Lithium Ion Batteries: Fundamentals and Performances*; Wakihara, M., Yamamoto, O., Eds.; Wiley-VCH: New York, 1999; p 127.

(4) Peled, E. In *Lithium Batteries*; Gabano, J. P., Ed.; Academic Press: New York, 1983.

(5) Peled, E.; Golodnitsky, D.; Menachem, C.; Bar-Tow, D. *J. Electrochem. Soc.* **1998**, *145*, 3482.

(6) Aurbach, D.; Levi, M. D.; Levi, E.; Schechter, A. *J. Phys. Chem. B* **1997**, *101*, 2195.

10.1021/ja0164529 CCC: $20.00
Published on Web 11/02/2001

Regarding the solvent-reduction mechanisms, for example for EC or PC, Dey[7] initially proposed a two-electron reduction process, bringing about a precipitate in organic electrolyte, Li_2CO_3, and ethylene or propylene gas. After extensive studies of solvent- and salt-reduction processes in the 1990s, Aurbach et al. concluded that lithium alkyl dicarbonate [$(CH_2OCO_2Li)_2$] and ethylene gas resulting from a one-electron reduction process of EC are the dominant products; however, the dicarbonate is highly sensitive to trace water and will react rapidly with it to form Li_2CO_3.[8,9] Shu et al.[10] suggested that both the one- and two-electron processes are involved. Naji et al.[11] found that EC reduction takes place in two steps, first a two-electron process above 0.8 V (versus Li^+/Li), resulting in an inorganic product Li_2CO_3, and second, a one-electron process giving rise to the two organic lithium bicarbonate compounds, $(ROCO_2Li)_2$ (R $= CH_2, CH_2CH_2$). More details about major experimental results before 1998 are given in a recent review paper.[12]

The EC/PC concentration dependence of the film components on the electrode surface was found by Aurbach et al.,[6,13] for example, at low EC (EC/DMC 1:5 in volume) concentration, the surface film main component is Li_2CO_3, while the products distribution shifts more and more toward lithium ethylene dicarbonate as the EC concentration increases. The suggested mechanisms for this phenomenon are the two-electron path,

$$EC + 2e^- + Li^+ \rightarrow C_2H_4\uparrow + (CO_3Li)^- \quad (1)$$

$$(CO_3Li)^- + Li^+ \rightarrow Li_2CO_3 \quad \text{at low EC concentration} \quad (2)$$

$$(CO_3Li)^- + Li^+ + EC \rightarrow (CH_2OCO_2Li)_2 \quad \text{at high EC concentration} \quad (3)$$

where the solvent concentration dependence was ascribed to the secondary reaction of $(CO_3Li)^-$ or $(CO_3)^{2-}$. Yang et al.[14] also investigated the passive film composition on the carbon anode surface in contact with an EC-based electrolyte, using FTIR and mass spectroscopy. They observed that the passive film contains chiefly $(CH_2OCO_2Li)_2$ not only for a single EC solvent but also for binary EC/DMC solvents (volume ratio 1:1, 1:3, 3:1,1 M lithium salt) and EC/DEC (1:1) regardless of the EC concentration.

Very recently, Aurbach et al.[15,16] employed FTIR and XPS techniques to study the surface film on freshly prepared lithium electrodes. Although the investigations were conducted on a lithium-metal anode, electrolyte reduction reactions on carbon surfaces are comparable to those on lithium metal, since the potential difference between metallic lithium and fully lithiated carbon is very small. Besides the confirmation that $(CH_2OCO_2Li)_2$ is the leading product in EC-based electrolyte solutions (EC/DMC, EC/DEC 1:1) and its secondary reaction with H_2O gives Li_2CO_3, an interesting finding is the XPS detection of a new surface species containing C−Li bonds, that is, Li carbides, $LiCH_2CH_2OCO_2Li$. The suggested reaction pathway for the new component is a two-electron reduction process, that is,

$$EC + 2e^- + 2Li^+ \rightarrow LiCH_2CH_2OCO_2Li\downarrow \quad (4)$$

This product appears also plausible especially at the inner side of the SEI film, close to the anode, as confirmed by another recent XPS results on highly oriented pyrolytic graphite (HOPG) (EC/DMC, 1:2 in volume).[17] Both Li_2CO_3 and $(ROCO_2Li)_2$ were also found on different HOPG sections.[17]

In contrast to the abundant experimental studies on the relevant topics of SEI film formation and characterization, only few theoretical studies can be found. On the basis of semiempirical MNDO and Hartree−Fock calculations, Endo et al.[18,19] claimed that the initial reaction was an electron transfer from the anode to the lithium-ion-coordinated solvent molecules, instead of being a transfer to isolated solvent molecules, because the former reduction to the open radical anion is exothermic, whereas the latter is endothermic. DFT and classical transition-state theory calculations for the model system, EC + one nucleophile (CH_3O^-),[20] supported the two-electron reduction process suggested by Aurbach et al.[6] In summary, although EC/PC reduction mechanisms are partially identified and some experimental facts are also at least partially understood, the details of the reduction chemistry are still highly debated subjects,[21−23] and there still remain a number of fundamental questions from theoretical and technological viewpoints that the present article intends to address. Reductive decomposition reactions of EC and the supermolecules $Li^+(EC)_n$ are investigated in the present paper by DFT and DFT-based polarized continuum model approaches. On the basis of these, several important questions are discussed. For example, does the EC molecule undergo one- and two-electron reduction processes? How do the salt and solvent affect the EC reduction mechanism? Do the reduction products of EC have solvent concentration dependence? If so, does it depend on the formation of $(CO_3Li)^-$ or on its secondary reaction as claimed by Aurbach et al.? [15,16] Capturing such microscopic details at the molecular level will be more helpful to understand the SEI surface chemistry and to design optimum electrolyte solutions. The calculated results are also compared with the available experimental findings with respect to the solvent-reduction potential and SEI constituents.

Computational Details

The use of standard ab initio correlation methods for the computation of large supermolecules is still too expensive; hence, the calculations were performed with the hybrid DFT method, B3PW91, as implemented in Gaussian 98,[24] hybrid exchange functional Becke3,[25] and correlation functional PW91.[26−28] The S^2 expectation values for the open-shell species in the present study are found nearly identical to the exact value. Therefore the B3PW91 method is also reliable for the open-shell species involved, as other hybrid DFT methods work well for open-shell molecules.[29,30] The geometries are fully optimized with a 6-311++G-

(7) Dey, A. N.; Sullivan, B. S. *J. Electrochem. Soc.* **1970**, *117*, 222.
(8) Aurbach, D.; Ein-Eli, Y.; Zaban, A. *J. Electrochem. Soc.* **1994**, *141*, L1.
(9) Aurbach, D.; Ein-Eli, Y.; Chusid, O.; Carmeli, Y.; Babai, M.; Yamin, H. *J. Electrochem. Soc.* **1994**, *141*, 603.
(10) Shu, Z. X.; McMillan, R. S.; Murray, J. J. *J. Electrochem. Soc.* **1993**, *140*, 922.
(11) Naji, A.; Ghanbaja, J.; Humbert, B.; Willmann, P.; Billaud, D. *J. Power Sources* **1996**, *63*, 33.
(12) Arora, P.; White, R. E.; Doyle, M. *J. Electrochem. Soc.* **1998**, *145*, 3647.
(13) Aurbach, D.; Moshkovich, M.; Cohen, Y.; Schechter, A. *Langmuir* **1999**, *15*, 2947.
(14) Yang, C. R.; Wang, Y. Y.; Wan, C. C. *J. Power Sources* **1998**, *72*, 66.
(15) Schechter, A.; Aurbach, D.; Cohen, H. *Langmuir* **1999**, *15*, 3334.
(16) Aurbach, D. *J. Power Sources* **2000**, *89*, 206.
(17) Bar-Tow, D.; Peled, E.; Burstein, L. *J. Electrochem. Soc.* **1999**, *146*, 824.
(18) Endo, E.; Ata, M.; K.Tanaka; K. Sekai *J. Electrochem. Soc.* **1998**, *145*, 3757.
(19) Endo, E.; Tanaka, K.; Sekai, K. *J. Electrochem. Soc.* **2000**, *147*, 4029.
(20) Li, T.; Balbuena, P. B. *Chem. Phys. Lett.* **2000**, *317*, 422.
(21) Ein-Eli, Y. *Electrochem. Solid-State Lett.* **1999**, *2*, 212.
(22) Chung, G.-C.; Kim, H.-J.; Yu, S.-I.; Jun, S.-H.; Choi, J.-W.; Kim, M.-H. *J. Electrochem. Soc.* **2000**, *147*, 4391.
(23) Zhang, X. R.; Pugh, J. K.; P. N. Ross, J. *Electrochem. Solid-State Lett.* **2001**, *4*, A82.

(d,p) basis set for the small systems, such as EC and $Li^+(EC)$, whereas 6-31G(d) is used for larger systems, $Li^+(EC)_n$ ($n = 2-4$). Single-point energies have also been calculated at the B3PW91/6-311++g(d,p) level for the systems containing two and more solvent molecules. To confirm the transition states and make zero-point energy (ZPE) corrections, frequency analyses are done with the correspondent basis sets. If not noted otherwise, relative energies refer to those with ZPE correction, and enthalpies and Gibbs free energies are calculated at 298.2K. Charges are calculated by fitting the molecular electrostatic potential (CHELPG method).[31]

Besides the supermolecule model, explicitly incorporating the local solvent effect, the bulk solvent effect is also considered as a macroscopic and continuum medium using the polarized continuum models (PCM). Specifically, the self-consistent isodensity PCM (SCIPCM)[32] implemented in Gaussian 94 is applied to the isolated EC molecule. The standard dielectric version D-PCM[33-35] and the conductor variant C-PCM[36] implemented in Gaussian 98 are applied to $Li^+(EC)_n$($n = 1-2$) system. In these models, the variation of the free energy when going from gas to solution consists of nonelectrostatic (cavitation energy, dispersion energy, and repulsion energy) and electrostatic energy terms, whose sum is referred to as W_0.[35,37] To be consistent for the reaction intermediates and transition states, the conventional set of Pauling radii[35] was used together with 60 tesserae per sphere for D-PCM and C-PCM calculations.

Results and Discussions

Supermolecular Models. It is important to choose a reliable model that could describe the practical situation in the electrolyte solutions of lithium ion batteries, that is, the local solvent structure around the lithium cation. For this end, a series of supermolecules, $Li^+(EC)_n$ ($n = 1-5$), were fully optimized. For $Li^+(EC)_2$, two nearly degenerate structures were located. One is a pseudo-planar structure, in the other two EC ligands are perpendicular to each other. For $Li^+(EC)_3$, the EC molecules are trigonal planar, pseudo-tetrahedral for $Li^+(EC)_4$, and trigonal bipyramidal for $Li^+(EC)_5$. The coordinated EC molecules nearly hold C_2 symmetry of the isolated EC, and the C=O bond slightly stretches by about 0.03 Å while the C−O bond contracts by 0.04 Å as compared with the isolated EC. Table 1 summarizes the binding characteristics, that is, the average bond distances (r) from the lithium cation to the carbonyl oxygen, average binding energy (ΔE), the heats of formation (ΔH_r), and Gibbs free energies of formation (ΔG_r) for these supermolecules. r increases with the number of EC molecules. Although the formation reaction for $Li^+(EC)_5$ is also exothermic, instead of endothermic as predicted with HF/6-31G*,[38] its Gibbs free energy of formation (ΔG) is positive. Thereby, we conclude that the leading component is the four-coordinated complex, $Li^+(EC)_4$. The result agrees with the conclusion from Raman intensity data[38] and classical molecular dynamics simulations.[39] Therefore, it may be reasonable to use the supermolecules $Li^+(EC)$ and $Li^+(EC)_4$ to model the reduction reaction center at low EC and high EC concentration, respectively.

Table 1. Li^+−O Distances (r/Å), Average Binding Energies (ΔE, kcal/mol), Heats of Reaction (ΔH_r, kcal/mol), and Gibbs Free Energies of Reaction (ΔG_r, kcal/mol) at 298.2 K, Calculated by B3PW91/6-31G(d)

reactions	r[a]	ΔE[b]	ΔH_r[c]	ΔG_r
$Li^+ + EC \rightarrow Li^+(EC)$	1.764	49.2	−50.6	−45.0
$Li^+(EC) + EC \rightarrow Li^+(EC)_2$	1.814	43.5	−38.5	−30.8
$Li^+(EC)_2 + EC \rightarrow Li^+(EC)_3$	1.893	36.9	−24.2	−12.7
$Li^+(EC)_3 + EC \rightarrow Li^+(EC)_4$	1.965	31.0	−13.9	−5.9
$Li^+(EC)_4 + EC \rightarrow Li^+(EC)_5$	2.088	26.8	−5.8	9.2

[a] Average bond lengths from Li^+ to the carbonyl oxygen of EC. [b] $\Delta E = -\{E[Li^+(EC)_n] - nE[(EC)] - E(Li^+)\}/n$. [c] $\Delta H_r = H[Li^+(EC)_n] - H[Li^+(EC)_{n-1}] - H(EC)$, the same definition for ΔG_r.

Reductive Dissociation of EC (1). The EC planar C_{2v} and nonplanar C_2 symmetry structures have been located using B3PW91, B3LYP,[25] and MP2/6-311++G(d,p) methods. The calculated characteristics of EC together with those determined from crystal structure[40] are listed in Table 2. Except for the dihedral angle, satisfactory consistency exists among the bond lengths and bond angles from different theoretical methods, which also agree very well with the measured data. In line with the early work[40] and further confirmation[41-43] about the crystal structure, density functional as well as ab initio methods, HF (not shown here) and MP2, predict that the EC ground state is a nonplanar structure with C_2 symmetry instead of a planar one of C_{2v} symmetry as obtained by Klassen et al.[38] and Blint[44] with HF/6-311++G(d,p) and HF/D95V** methods implemented in Gaussian 92 and 90, respectively. The methylene (CH_2) group bends from CO_3 plane by 10°, 8°, and 3° with MP2, B3PW91, and B3LYP methods, respectively. Very early experimental work of Angell,[45] however, showed that the EC structure is planar in the liquid and gaseous states. Although the energy barrier is only about 0.3 kcal/mol, the planar geometry with C_{2v} symmetry is indeed a transition state connecting the two configurations of C_2 symmetry, which is confirmed by the sole imaginary frequency and primary intrinsic reaction coordinate (IRC) calculation. Therefore we strongly *suggest* that the stable structure of EC is nonplanar.

The potential energy and Gibbs free energy profile of reductive dissociation for isolated EC is shown in Figure 1, and specific data is listed in Table 3. The EC molecule has a negative adiabatic electron affinity (EA) of 7.6 kcal/mol in gas phase. Population analysis indicates that the excess electron mainly

(24) Frisch, M. J.; Trucks, G. W.; Schlegel, H. B.; Scuseria, G. E.; Robb, M. A.; Cheeseman, J. R.; Zakrzewski, V. G.; Montgomery, J. A., Jr.; Stratmann, R. E.; Burant, J. C.; Dapprich, S.; Millam, J. M.; Daniels, A. D.; Kudin, K. N.; Strain, O. F. M. C.; Tomasi, J.; Barone, B.; Cossi, M.; Cammi, R.; Mennucci, B.; Pomelli, C.; Adamo, C.; Clifford, S.; Ochterski, J.; Petersson, G. A.; Ayala, P. Y.; Cui, Q.; Morokuma, K.; Malick, D. K.; Rabuck, A. D.; Raghavachari, K.; Foresman, J. B.; Ciolovski, J.; Ortiz, J. V.; Stefanov, V. V.; Liu, G.; Liashensko, A.; Piskorz, P.; Komaroni, I.; Gomperts, R.; Martin, R. L.; Fox, D. J.; Keith, T.; Al-Laham, M. A.; Peng, C. Y.; Nanayakkara, A.; Gonzalez, C.; Challacombe, M.; Gill, P. M. W.; Johnson, B.; Chen, W.; Wong, M. W.; Andres, J. L.; Head-Gordon, M.; Replogle, E. S.; Pople, J. A. *Gaussian 98;* Gaussian Inc.: Pittsburgh, PA, 1998.
(25) Becke, A. D. *J. Chem. Phys.* **1993**, *98*, 5648.
(26) Perdew, J. P. In *Electronic Structure of Solids*; Ziesche, P., Eschrig, H., Eds.; Akademie Verlag: Berlin, 1991.
(27) Burke, K.; Perdew, J. P.; Wang, Y. *Electronic Density Functional Theory: Recent Progress and New Directions*; Plenum: New York, 1998.
(28) Perdew, J. P.; Burke, K.; Wang, Y. *Phys. Rev. B* **1996**, *54*, 16533.
(29) Baker, J.; Scheiner, A. C.; Andzelm, J. J. *Chem. Phys. Lett.* **1993**, *216*, 380.
(30) Baker, J.; Muir, M.; Andzelm, J. J. *J. Chem. Phys.* **1995**, *102*, 2065.
(31) Breneman, C. M.; Wiberg, K. B. *J. Comput. Chem.* **1990**, *11*, 361.
(32) Foresman, J. B.; Keith, T. A.; Wiberg, K. B.; Snoonian, J.; Frisch, M. J. *J. Phys. Chem.* **1996**, *100*, 16098.
(33) Miertus, S.; Scrocco, E.; Tomasi, J. *Chem. Phys.* **1981**, *55*, 117.
(34) Miertus, S.; Tomasi, J. *Chem. Phys.* **1982**, *65*, 239.
(35) Cossi, M.; Barone, V.; Cammi, R.; Tomasi, J. *Chem. Phys. Lett.* **1996**, *255*, 327.
(36) Barone, V.; Cossi, M. *J. Phys. Chem. A* **1998**, *102*.
(37) Arnaud, R.; Adamo, C.; Cossi, M.; Milet, A.; Vallee, Y.; Barone, V. *J. Am. Chem. Soc.* **2000**, *122*, 324.
(38) Klassen, B.; Aroca, R.; Nazri, M.; Nazri, G. A. *J. Phys. Chem. B* **1998**, *102*, 4795.
(39) Li, T.; Balbuena, P. B. *J. Electrochem. Soc.* **1999**, *146*, 3213.
(40) Brown, C. J. *Acta Crystallogr.* **1954**, *7*, 92.
(41) Wang, J.; Britt, C. O.; Boggs, J. E. *J. Am. Chem. Soc.* **1965**, *87*, 4950.
(42) Fortunato, B.; Mirone, P.; Fini, G. *Spectrochim. Acta* **1971**, *27A*, 1917.
(43) Pethrich, R. A.; Wilson, A. D. *Spectrochim. Acta* **1974**, *30A*, 1073.
(44) Blint, R. J. *J. Electrochem. Soc.* **1995**, *142*, 696.
(45) Angell, C. L. *Trans. Faraday Soc.* **1956**, *52*, 1178.

Table 2. Characteristics of Ethylene Carbonate Calculated with DFT and ab Initio Methods (distances in Å, Angles in deg, Energies in au, Frequencies in cm^{-1})

	measured[a]	C_{2v} B3PW91/A[c]	C_2 B3PW91/A	C_{2v} B3LYP/A	C_2 B3LYP/A	C_{2v} MP2/A	C_2 MP2/A
C1═O1	1.15	1.187	1.187	1.188	1.188	1.193	1.193
C1−O2[b]	1.33	1.353	1.356	1.359	1.361	1.360	1.364
C2−O2[b]	1.40	1.426	1.429	1.434	1.437	1.429	1.433
C2−C2	1.52	1.538	1.525	1.543	1.530	1.541	1.522
∠O1C1O2	124.1	124.7	124.9	124.8	124.9	124.6	124.9
∠C1O2C2	109	110.7	109.2	110.8	109.4	110.4	108.3
∠O1C1O2C2		180.0	−171.5	180.0	−176.7	180.0	−169.7
imaginary frequency[d]		−132		−128		−177	
E[e]		−342.293391	−342.293910	−342.428207	−342.428661	−341.552284	−341.553949

[a] From ref 40. [b] C1, C2 refer to carbonyl and ethylene carbon respectively; O1, O2 to carbonyl and ethereal oxygen. [c] A: 6-311++G(d,p). [d] No scaling. [e] Including zero-point energy correction.

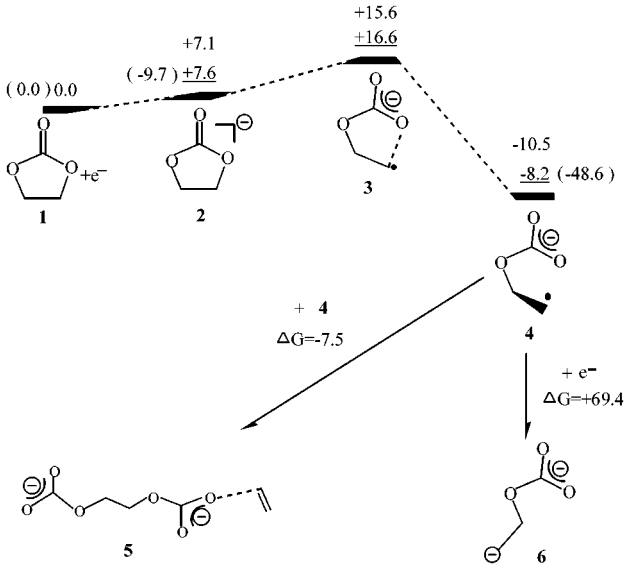

Figure 1. Potential energy (underlined data) and Gibbs free energy profile at 298.15 K for EC reductive dissociation calculated with B3PW91/6-311++G(d,p). The data in parentheses refer to SCI−PCM-B3PW91/6-311++G(d,p).

Table 3. Relative Energies, Enthalpies, and Free Energies (in kcal/mol), Dipole Moment (D/Debye) for Stationary Points and Imaginary Frequency (IF/cm^{-1}) for Transition States

structures	ΔE[a]	ΔE_0[b]	ΔH[c]	ΔG[d]	D	IF
1	0.0 (0.0)	0.0	0.0	0.0	5.6	
2	8.0 (−9.7)	7.6	7.6	7.1	6.9	
3 (TS,2↔4)	19.8	16.6	16.8	15.6	4.2	−1041
4	−3.2 (−48.6)	−8.2	−7.1	−10.5	5.5	
5/2	−13.5	−16.5	−14.9	−14.3	9.5	
6	65.8	60.2	61.2	+58.5	12.6	

[a] ΔE (B3PW91/6-311++G(d,p)), the data in the parenthesis from SCIPCM-B3PW91/6-311++G(d,p). [b] ΔE_0 (B3PW91/6-311++G(d,p)) + ΔZPE (B3PW91/6-311++G(d,p)). [c] ΔH (298.2 K) (B3PW91/6-311++G(d,p)). [d] ΔG (298.2 K) (B3PW91/6-311++G(d,p).

delocalizes over the CO_3 group; however, the anion **2** still retains C_2 symmetry. The energy barrier for the ring opening of EC anion **2** is 9.0 kcal/mol. The formation of radical anion **4** releases 15.8 kcal/mol as compared with anion **2**, and the unpaired electron mainly locates on the leaving carbon atom in **4**. The dimerization of **4** to **5** is thermodynamically favorable with $\Delta G = -7.5$ kcal/mol, whereas the further reduction of **4** is forbidden with quite high positive $\Delta G = +69.4$ kcal/mol.

The solvent effect on the EC reduction path was addressed by re-optimizing the geometries of **1**, **2**, **4**, and **6** with SCIPCM-B3PW91/6-311++G(d,p) method in EC bulk solvent (dielectric constant $\epsilon = 89.78$ at 298.2 K). The solvent field significantly stabilizes both **2** and **4**. The EC adiabatic EA becomes positive in solvent medium (−8.0 in gas phase vs 9.7 kcal/mol in bulk solvent without ZPE correction), and much more energy is released by formation of **4** (−3.2 vs −48.6 kcal/mol). The most interesting aspect is that **6** tends to break into ethylene gas and a CO_3^{2-} group. Although the optimized structure was not obtained with $\epsilon = 89.78$, we observed a bond rupture that the C−O2 bond (ethereal oxygen, same notation below) stretches from 1.50 in the gas phase to 1.6 Å at $\epsilon = 20$, and further to 3.2 Å at $\epsilon = 40$. Therefore, in gas phase the reduction of EC is thermodynamically forbidden, whereas it is possible that EC undergoes one- as well as two-electron reduction processes in bulk solvent.

Effect of Li^+ on EC Reductive Decomposition, Li^+(EC) (7). To evaluate the effect of Li^+ cation, the reduction mechanisms of supermolecule **7** are investigated (Figure 2a). Relative energies for all stationary points are collected in Table 4. The potential energy surface and Gibbs free energy surface profiles are shown in Figure 2a together with selected structural data. In sharp contrast to an isolated EC molecule, Li^+(EC) becomes much more easily reduced, bringing about an ion-pair intermediate **10**. Although Li^+ has much higher electron affinity than the EC molecule in gaseous phase (+5.55 vs −0.3ev, physical scale) at B3PW91/6-311++G(d,p) level, the reduction intermediate **10** has 2.7 kcal/mol lower energy than the other intermediate **8**, an electron was transferred to EC in **10** and to Li^+ in **8** respectively. In **10**, the unpaired spin density is mainly located at the carbonyl carbon with a coefficient of 0.77, whereas a 0.16 coefficient is found at the carbonyl oxygen. The CO_3 group carries an overall charge of −1.31e, which is 0.76e more negative than in **7** (−0.55e). The C−O2 bond on the side to which lithium cation shifts is quite loose (bond length 1.583 Å), the other bonds more or less stretched relative to **7**, and the CO_3 group does not keep the planar structure. It seems likely that the carbonyl C changes from sp^2 in **7** to nearly sp^3 hybridization in **10**. In the case of **8**, the unpaired electron locates at the lithium atom with a coefficient of 1.08. Besides a little stretch of C═O bond by 0.02 Å, the structure of the EC moiety in **8** keeps rather close to an isolated one.

Homolytic ring opening could happen to both **10** and **8**, leading to a radical anion coordinated with lithium cation. The opening in **10** through a transition state **11** faces a barrier of 11.5 kcal/mol, which is 5.5 kcal/mol higher than that corresponding to **8**. The unpaired spin density in **11** is mainly located at the leaving carbon (C2) and at the carbonyl carbon (C1) with coefficients of 0.45 and 0.54, respectively, while in **9** it is mainly located at Li and C2 with 0.51 and 0.40, respectively. In **9**, Li bears a positive charge of +0.23e and the CO_3 group a more negative charge (−0.63e in **9**, −0.52e in **8**), which shows that partial charge is being transferred from Li to the CO_3 group,

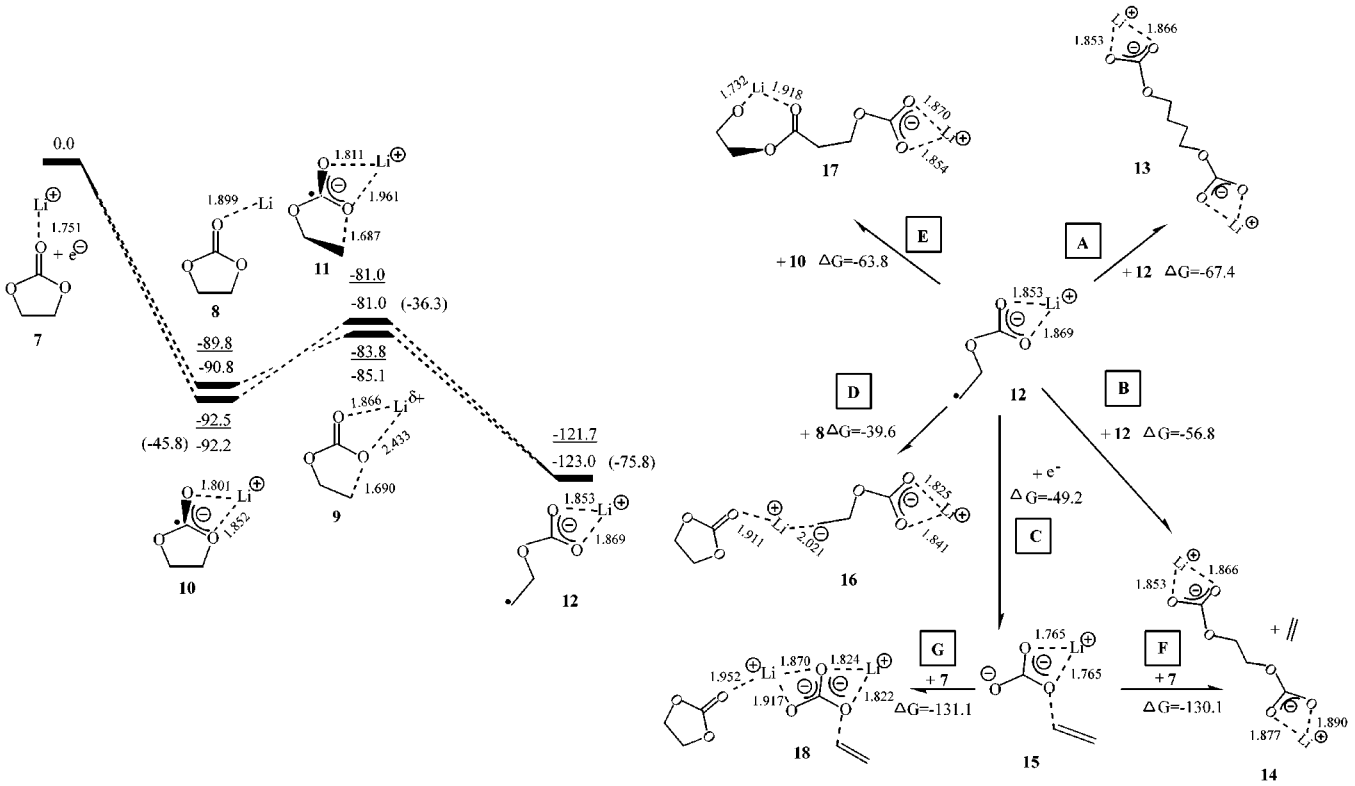

Figure 2. (a) Potential energy (underlined data) and Gibbs free energy profile at 298.15 K for the reductive dissociation process of Li^+(EC) calculated with B3PW91/6-311++G(d,p) methods. The data in the parentheses refer to C−PCM-B3PW91/6-311++G(d,p)//B3PW91/6-311++G-(d,p). (b) Termination reactions of carbonate radical anion coordinated with lithium cation for the model Li^+(EC).

Table 4. Relative Energies, Enthalpies, and Gibbs Free Energies (in kcal/mol), Charge (*q*/*e*), Main Coefficients of Spin Densities (SD/*e*) for Stationary Points and Imaginary Frequency (IF/cm^{-1}) for Transition States in the Case of Li^+(EC)

					q[e]		SD[f]			
structures	ΔE^a	$\Delta E_0{}^b$	ΔH^c	ΔG^d	Li	CO_3	C1	Li	C2	IF
7	0.0	0.0	0.0	0.0	+0.97	−0.55				
8	−89.1	−89.8	−90.2	−90.8	−0.21	−0.52		1.1		
9 (TS, 8↔12)	−80.4	−83.8	−83.5	−85.1	+0.23	−0.63		0.51	0.40	−783
10	−90.5	−92.5	−92.6	−92.2	+0.83	−1.3	0.77			
11(TS, 10↔12)	−77.1	−81.0	−81.1	−81.0	+0.75	−0.78	0.54		0.45	−906
12	−117.2	−121.7	−120.9	−123.0	+0.83	−1.2			1.2	
13/2	−161.7	−162.2	−162.0	−156.7						
14/2	−152.5	−154.6	−153.7	−151.4						
15	−163.5	−168.9	−167.4	−172.6						
16/2	−129.1	−130.6	−130.2	−126.7						
17/2	−144.3	−145.5	−145.5	−139.5						
18/2	−154.4	−156.4	−155.9	−151.8						

[a] ΔE_{tot} (B3PW91/6-311++G(d,p)). [b] ΔE_{tot} (B3PW91/6-311++G(d,p)) + ΔZPE(B3PW91/6-311++G(d,p)). [c] ΔH (298.2 K) (B3PW91/6-311++G(d,p)). [d] ΔG (298.2 K) (B3PW91/6-311++G(d,p). [e] Charges from ESP fit by Chelpg. [f] Mulliken spin density population, C1 and O1 refer to carbonyl group, C2 leaving carbon of ring-opening reactions.

favoring the ring opening. The transition-state characteristics of **9** and **11** connecting each **8** and **10** with **12** are confirmed by primary IRC calculations as well as by identification of imaginary frequencies corresponding to relevant vibrational modes. Formation of the primary radical anion **12** results in much more energy releasing, −121.7 kcal/mol relative to **7**.

Does the structural change happen to **7**, i.e, before the electron transfer? By scanning the bond length of C2−O2, the results indicate that the energy of **7** will continuously increase by over 60.0 kcal/mol until 2.9 Å, the possible barrier of which is 5 times higher that of **10**. Therefore, we could conclude that the transferred electron induces the rearrangement of Li^+(EC), as in the cases of **8** and **10**, and that on the contrary it is unlikely that the structural change would induce the electron transfer.

We have examined possible termination ways of radical anion **12** as shown in Figure 2b. One would expect that the direct barrierless combination of **12** (path **A**) via radical center to form lithium butylene dicarbonate, $(CH_2CH_2OCO_2Li)_2$, **13**, would be the most probable reaction, a path that was questioned by Aurbach et al.,[46] but confirmed by Naji et al.[11] using transmission electron microscopy (TEM) and FTIR to characterize a SEI film in a $LiClO_4$−EC electrolyte, and suggested by Bar-Tow et al.[17] Its Gibbs free energy of reaction ($\Delta G = -67.4$ kcal/mol) is the most favorable among the involved reactions. Nucleophilicly attacking the radical center by oxygen, radical anion **12** could undergo another dimerization probably without barrier (transition state has not been found, path **B**), bringing about lithium ethylene dicarbonate, $(CH_2OCO_2Li)_2$, **14**, which is the most common product found experimentally[11,15−17,46] and usually considered as a dominant component[15,16] on the anode

(46) Aurbach, D.; Weissman, I.; Schechter, A.; Cohen, H. *Langmuir* **1996**, *12*, 3991.

Table 5. Relative Energies, Enthalpies, and Free Energies (in kcal/mol), Charge (*q*/*e*), Main Coefficients of Spin Densities (SD) for Stationary Points and Imaginary Frequency (IF/cm^{-1}) for Transition States in the Case of $Li^+(EC)_2$

						q		SD				
structures	ΔE^a	$\Delta E(0)^b$	$\Delta E_0{}^c$	ΔH^d	ΔG^e	Li	CO_3	C1	Li	C2	O1	IF
19	0.0	0.0	0.0	0.0	0.0	+0.96	−0.50					
20	−57.1	−58.6	−61.4	−61.2	−61.8	−0.30	−0.42		0.90			
21	−68.0	−70.0	−72.4	−72.7	−70.6	+0.78	−1.2	0.67	0.08		0.15	
22	−63.9	−65.4	−68.2	−69.0	−63.1	+0.81	−0.81	0.29			0.12	
23(TS,20↔25)	−50.1	−54.1	−58.8	−58.7	−58.8	+0.13	−0.64		0.58	0.29		−789
24(TS,21↔25)	−53.9	−57.7	−61.4	−61.7	−60.1	+0.71	−1.1	0.43	0.10	0.41	0.12	−916
25	−92.6	−97.2	−102.3	−101.6	−102.4	+0.71	−1.1			1.1		
26	−66.0	−70.9	−80.0	−80.2	−77.2	+0.76	−1.2	0.66			0.17	
27(TS,26↔28)	−53.1	−59.8	−71.0	−71.1	−68.6	+0.69	−0.82	0.42	0.13	0.40	0.14	−907
28	−132.4	−137.4	−152.5	−151.8	−150.9	+0.72	−1.54					
29/2	−105.4	−106.8	−109.2	−109.0	−101.0							
30/2	−126.5	−128.5	−132.9	−132.3	−126.1							
31/2	−128.1	−129.9	−132.3	−131.8	−124.0							
32/2	−138.5	−139.1	−142.5	−142.7	−134.4							
33/2	−123.3	−123.6	−125.0	−125.5	−115.7							

[a] ΔE (B3PW91/6-31G(d)). [b] ΔE_0 (B3PW91/6-31G(d)) + ΔZPE (B3PW91/6-31G(d)). [c] ΔE_0 (B3PW91/6-311++G(d,p)//B3PW91/6-31G(d)) + ΔZPE(B3PW91/6-31G(d)). [d] ΔH, ΔE (B3PW91/6-311++G(d,p)//B3PW91/6-31G(d)) + $\Delta\Delta H$ (B3PW91/6-31G(d)). [e] ΔG,ΔE (B3PW91/6-311++G(d,p)//B3PW91/6-31G(d)) + $\Delta\Delta G$(B3PW91/6-31G(d).

surface. A third termination way is the further reduction by another electron transfer from the polarized electrode (path **C**), by which a weak complex **15** of ethylene gas and an unpaired nucleophilic carbonate anion ($LiCO_3^-$) are generated. Besides these three paths, of particular interest is the possibility of forming a species containing C−Li bonds (Li carbides) solvated by a EC molecule, **16**, $Li(CH_2)_2OCO_2Li$, via electron pairing between **12** and a reduction intermediate **8** (path **D**). The path is in line with recent discoveries using the XPS technique.[15,17] In accordance with the usual definition, the formation of the Li carbide species proceeds via a two-electron reduction mechanism like path **C**. However, the added electrons are distributed on the two separate species (**8** and **12**), instead of being added as a continuous process to one species as in **15**. Another possible way is the combination of **12** with the other reduction intermediate **10** also via electron pairing (path **E**) that generates a lithium organic salt with an ester group, $LiO(CH_2)_2CO_2(CH_2)_2OCO_2Li$, **17**.

Once the carbonate anion ($LiCO_3^-$) of **15** is formed, it may either nucleophilicly attack another Li^+(EC), **7**, to form lithium ethylene dicarbonate (path **F**), or being paired by Li^+ from **7** (path **G**), it may precipitate as insoluble inorganic lithium carbonate Li_2CO_3, **18**. The two paths are thermodynamically very competitive as shown by their almost identical Gibbs free energies of reaction (ΔG, −130.1 vs −131.1 kcal/mol).

Several points about the reductive dissociation of Li^+-coordinated EC could be drawn from the above results. The interplay of EC and Li^+ considerably increases the EC adiabatic EA up to quite high values, and decreases that of Li^+. The reductive decomposition of EC initially encounters an ion-pair intermediate **10**. It then homolytically cleavages via a 11.5 kcal/mol barrier to generate a radical anion, which will undergo secondary reactions by barrier-free self-dimerizing (paths **A** and **B**), further reduction (path **C**), electron pairing (path **D**, **E**) as well as ion-pairing processes.

Effect of One Unreactive Solvent Molecule, $Li^+(EC)_2$ (19). To evaluate the possibility of a coordinated solvent-molecule effect, the above reaction pathways were investigated for $Li^+(EC)_2$ (**19**). The corresponding data are summarized in Table 5 and the relative energy, Gibbs free energy, and selected structural information are shown in Figure 3, a and b. Besides the two types of reductive intermediates, **20** and **21**, corresponding to the reduction of either Li^+ or one of the EC molecules in **19**, there is a third intermediate, **22**, where the two EC molecules are equally reduced. Its energy lies between those of **20** and **21**. The adiabatic EAs of **19** reduced to **20** and **21** are considerably lower than those of **7** to **8** and **10** by 29 and 20 kcal/mol respectively according to B3PW91/6-311++G-(d,p)//B3PW91/6-31G(d). The EA difference between **20** and **21** is increased to 11.0 kcal/mol, compared to a value of 2.7 kcal/mol, corresponding to that between **8** and **10**. We could conclude that the supermolecule reduction at high EC concentration is not as favorable as that at lower concentration and that the reduction of Li^+ becomes much less favorable than that of the EC molecule.

Close inspection shows (Figure 3a) that the binding energies between Li^+(EC) and an additional EC molecule before and after reduction are much different, for example, 39.0 kcal/mol in **19**, whereas only 8.5 kcal/mol in **20** and 19.7 kcal/mol in **21**. This indicates that the interaction between Li^+(EC) and EC is significantly reduced after reductions of either EC or Li^+. Consequently, the distances between Li and the unreactive EC molecule stretch from 1.814 to 1.949 Å in **20** and to 1.931 Å in **21**. The weak interactions should be responsible for the smaller adiabatic EAs of **19** compared to that of **7**. Except for the additional EC molecule, the structure of the transition state **24** remains similar to that of **11**, and so does that of **23** with respect to that of **9**. The weak interaction between the unreactive EC and lithium results in 19.4 kcal/mol less energy release in **25** than in **12**. On the basis of the reduction intermediates **10** and **21**, radical anions **12** and **25** release more or less the same amount of energy, 29.2 and 29.9 kcal/mol, respectively.

How does the unreactive solvent affect the termination reactions of the radical anion **25**? Compared with the case of Li^+(EC), the Gibbs free energies of reaction ΔG's are generally increased (less negative). Comparing Figures 2b and 3b, the ΔG increments for paths **C** and **D** are only 0.7 and 1.7 kcal/mol, respectively, whereas they are 3.4 and 5.4 kcal/mol for paths **A** and **E**, respectively. A considerable increase is found for path **B**, 9.4 kcal/mol. As to the further reaction of $(CO_3Li)^-$ with a supermolecule, ΔG in Figure 3b is much higher, by about 30.0 kcal/mol, for paths **F** and **G**, with path **G** being a little less favorable than path **F** (−97.0 vs −101.1 kcal/mol).

On the basis of the Gibbs free energies of reaction at 298.15 K, paths **A** and **E** (Figure 3b) are thermodynamically the two most favorable termination ways for both radical anions **12** and

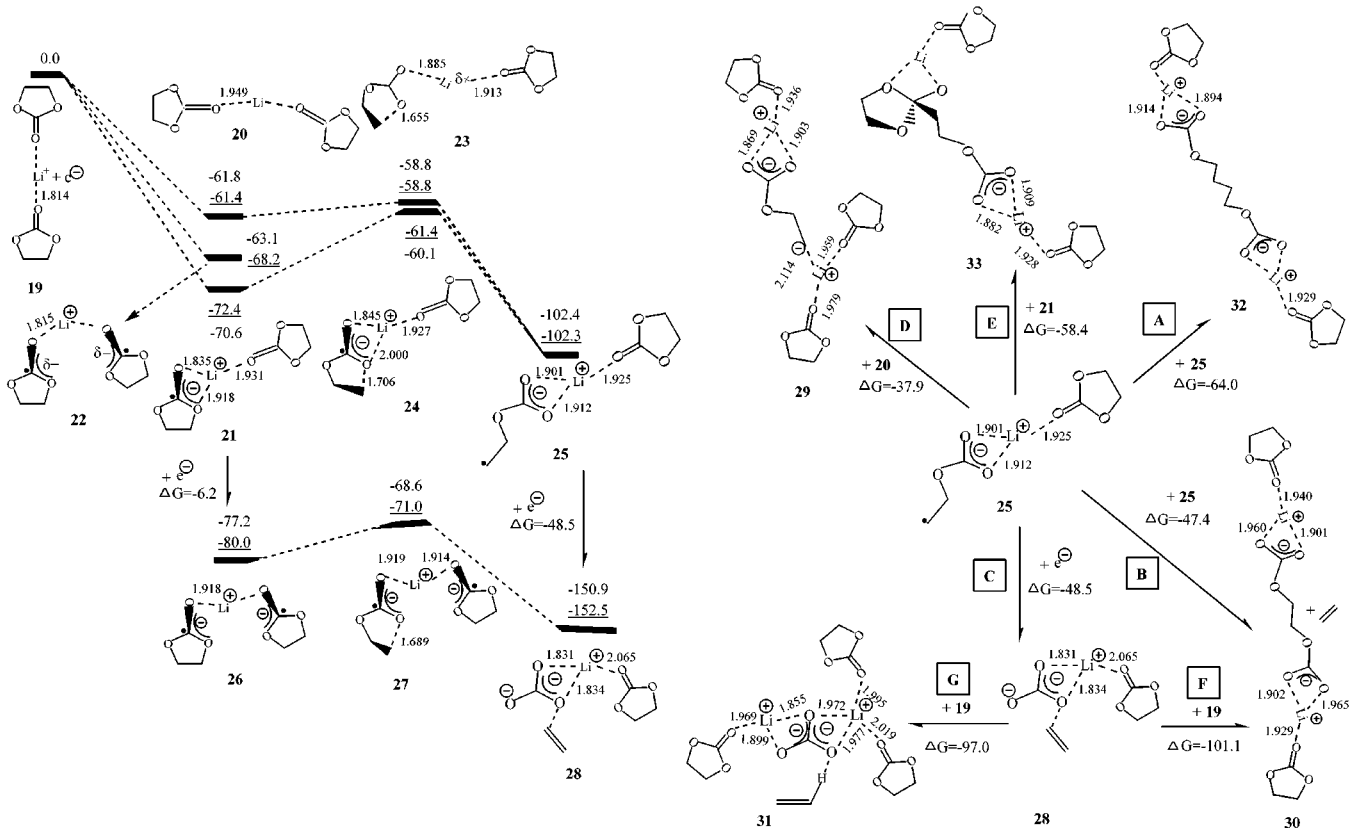

Figure 3. (a) Potential energy (underlined data) and Gibbs free energy profile at 298.15 K for the reductive dissociation process of $Li^+(EC)_2$ calculated with B3PW91/6-311++G(d,p)// B3PW91/ 6-31G(d) method. (b) Termination paths for the radical anion from the reductive dissociation process $Li^+(EC)_2$ calculated with B3PW91/6-311++G(d,p)//B3PW91/6-31G(d) method.

25. Despite being also a dianionic species, lithium butylene dicarbonate $(CH_2CH_2OCO_2Li)_2$ (product of path **A**), is more soluble in organic solvent than lithium ethylene dicarbonate, $(CH_2OCO_2Li)_2$ (product of path **B**) due to its longer chain $-(CH_2)_4-$. Therefore, it will contribute less, if at all, to a solid SEI film. Actually, the difference between the calculated vibrational spectra of the two dicarbonates is also negligible. Therefore, it may be unlikely that the existence of lithium butylene dicarbonate can be clarified by FTIR. However, Aurbach et al.[46] found that the percentage of the alkyl carbon XPS peak around 285−286 eV is much higher than that expected for $(CH_2OCO_2Li)_2$ only. They attributed the stronger peak to that arising from the two lithium dicarbonates and claimed that path **A** on the Li surface perhaps takes place (in tetrabutylammonium salt solutions). The path **A** is also supported by the TEM study of Naji et al.,[11] where a radical anion from the decomposition of EC−$LiClO_4$ electrolyte is reorganized into two different lithium dicarbonate products with O/C ratios of 1.5 and 1.0 (the former refers to $(CH_2OCO_2Li)_2$ and the latter to $(CH_2CH_2OCO_2Li)_2$). Due to similar high-solubility reasons, it is not certain whether the organic product (path **E)**, $LiO(CH_2)_2CO_2(CH_2)_2OCO_2Li$, could considerably precipitate on the carbon electrode surface to passivate the electrode or not. To the best of our knowledge, experimental findings about path **E** have not been reported. Paths **B** and **C** are very competitive processes. Thermodynamically, the least favorable path is path **D**, forming a C−Li bond compound. However, it is worthwhile to note that C−Li bond containing compounds (Li carbides) were discovered by Aurbach et al.[15] (EC-DMC, 1:1, 1 M $LiAsF_6$) and by Bar-Tow et al.[17] using the XPS technique.

The reactions that involve unpaired lithium carbonate (**15** and **28)** are very sensitive to the basis set, that is, paths **C**, **F**, and **G**, especially path **C** (see Table 8). For example, path **C** has the lowest negative ΔG among the termination reactions of **25** at B3PW91/6-31G* level (−38.2, −41.0, −48.6, −63.0, and −67.6 kcal/mol for paths **C**, **D**, **B**, **E**, and **A**, respectively, as shown in Table 8), whereas it is decreased by 12.4 kcal/mol at B3PW91/6-311++G(d,p) level so that path **C** has even lower ΔG than path **D** and path **B**. Another interesting question is the temperature effect on ΔG for the several reaction paths, because of the wide range of temperatures for battery operation. In the range of 273.2−323.2 K, ΔG increases about 1.0 kcal/mol per 25 K for the investigated paths, with one exception of path **C** where ΔG nearly keeps constant.

We have also explored the possibility that a second electron transfer could be undertaken starting from **21**, as shown in Figure 3a. Two EC molecules are equally reduced in **26**, and the ground state is a triplet state. Its homolytic ring opening will encounter a triplet transition state **27**, resulting in a singlet product **28** to avoid potential energy surface crossing. Although the energy barrier of C−O bond cleavage for TS **27** as shown in Figure 3a, is even lower than the first electron-transfer process (9.0 vs 11.0 kcal/mol), the process of **21** to **26** thermodynamically is much less favorable than that of **25** to **28** (ΔG, −6.2 vs −48.5 kcal/mol). Therefore, this alternative path is less important in the two-electron reduction process than path **C**.

More Realistic Supermolecule Models for Solvent Effect-$Li^+(EC)_3$ (34) and $Li^+(EC)_4$ (43). Two more realistic supermolecule models, $Li^+(EC)_3$ and $Li^+(EC)_4$, are used to further investigate the solvent-reduction mechanisms. Relevant data are collected in Table 6 for $Li^+(EC)_3$ and $Li^+(EC)_4$. Profiles of the potential energy surface and Gibbs free energy surface are shown in Figures 4 and 5, respectively. Li^+ coordinates with O1 (carbonyl oxygen) as well as one of O2 (ethereal oxygen)

Table 6. Same Meaning as In Table 5 except for the Structures of $Li^+(EC)_3$ and $Li^+(EC)_4$ Models

						q		SD			
structures	ΔE	ΔE_0	$\Delta E(0)$	ΔH	ΔG	Li	CO_3	C1	Li	C2	IF
					$Li^+(EC)_3$						
34	0.0	0.0	0.0	0.0	0.0	+0.87					
35	−58.5	−60.2	−64.6	−64.5	−61.6	+0.71	−1.1	+0.71			
36(TS,35↔37)	−45.4	−49.2	−53.5	−53.4	−50.4	+0.67	−0.99	0.45		0.42	−916
37	−83.1	−87.2	−93.9	−92.9	−92.3	+0.73	−0.97			1.1	
38	−126.6	−131.4	−145.9	−144.9	−142.6	+0.72	−1.4				
39/2	−116.1	−118.3	−123.4	−122.2	−116.8						
40/2	−114.2	−116.8	−120.3	−119.4	−112.2						
41/2	−91.2	−92.9	−96.3	−95.5	−88.5						
42/2	−129.0	−129.6	−133.5	−133.0	−125.5						
					$Li^+(EC)_4$						
43	0.0	0.0	0.0	0.0	0.0	+0.91					
44	−53.4	−55.0	−59.0	−59.7	−51.4	+0.70	−0.93	0.67			
45(TS, 44↔46)	−39.7	−43.3	−48.8	−49.5	−41.4	+0.71	−0.68	0.43		0.44	−923
46	−76.3	−80.6	−86.9	−86.6	−81.5	+0.75	−0.94			1.1	
47	−46.2	−50.8	−64.8	−64.7	−62.1	+0.59	−1.1	0.68	0.12		
48(TS, 47↔49)	−37.4	−44.0	−59.8	−59.6	−58.0						−906
49	−117.4	−122.7	−138.2	−137.4	−133.2						

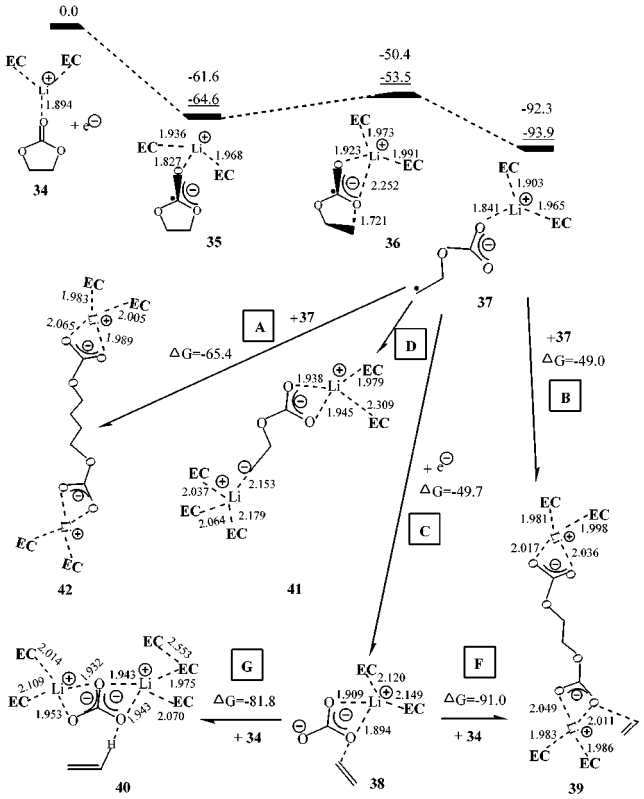

Figure 4. Potential energy (underlined data) and Gibbs free energy profile at 298.15 K for the reductive decomposition process of $Li^+(EC)_3$ calculated with B3PW91/6-311++G(d,p)// B3PW91/6-31G(d) method.

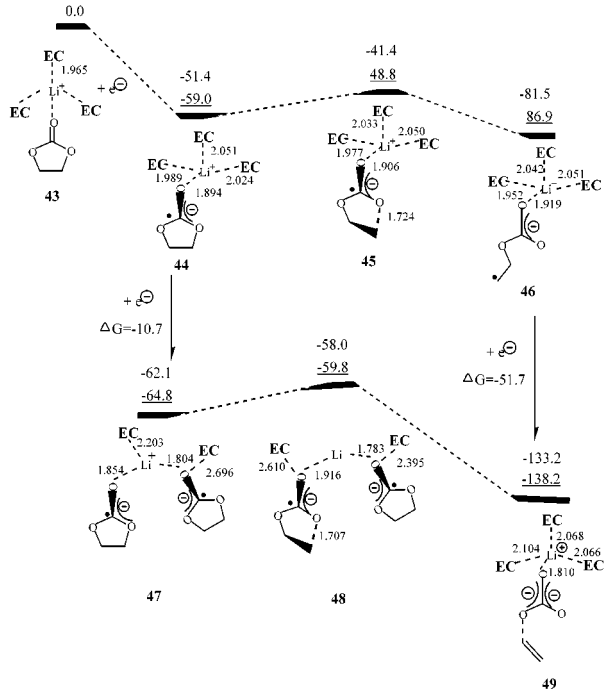

Figure 5. Potential energy (underlined data) and Gibbs free energy profile at 298.15 K for the reductive decomposition process of $Li^+(EC)_4$ with B3PW91/6-311++G(d,p)//B3PW91/6-31G(d) method.

of the reduced EC molecule in the reduction intermediates of $Li^+(EC)$ and $Li^+(EC)_2$, where the distances are 1.801/1.852 Å for **10** and 1.835/1.918 Å for **21**. But Li^+ moves far away from O2 (beyond 3 Å) and only coordinates with O1 in the $Li^+(EC)_3$ and $Li^+(EC)_4$ reduction intermediates **35** and **44** perhaps due to more $Li^+\cdots O{=}C$ interactions. Another clear effect of the solvent molecules on the reduced EC molecule is that the C−O2 bonds are not yet as loose as those in **10** and **21**, for example, the C−O2 bond lengths are, 1.577(**10**), 1.558(**21**), 1.470(**35**), and 1.459 Å (**44**). The adiabatic EAs for $Li^+(EC)_3$, **34**, and $Li^+(EC)_4$, **43**, are decreased further as compared with **19**, as well as the releasing energies of the radical anions **37** and **46**. As in the case of $Li^+(EC)_2$, the ring-opening energy barriers for the intermediates **35** and **44** via TS **36** and **45** still remain close to those of **10** and **21**, 11.1 and 10.2 kcal/mol, respectively.

To quantitatively discuss the trends of the adiabatic EAs of the supermolecules $Li^+(EC)_n$ ($n = 1-4$), Table S1 lists the energy levels and the main components of two of the lowest virtual KS orbitals with coefficients over 0.2, to which the dominant contribution comes from one of EC molecules and Li^+ respectively. Generally the energy levels of the two types of virtual orbitals increase with the number of coordinated EC molecules (n), but the differences between them, comparing systems n and $n + 1$, decrease with n, for example, 0.041, 0.024, and 0.022 au from $n = 1-4$ for the lowest virtual orbitals occupied by EC. It is well-accepted that the negatives of the energies of the virtual orbitals correspond to vertical electron affinities,[47] and thus this could explain the variations of EA

Table 7. Solvent Effect Calculated from C-PCM and D-PCM Models (Dielectric Constant $\epsilon = 89.78$; ΔG_{vac} and ΔG_{sol} Refer to the Gibbs Free Energy in the Gas Phase, and in the Solution Phase, Respectively; ΔW_0^D and ΔW_0^C to the Contribution from D-PCM and C-PCM-B3PW91LYP/6-311++G(d,p)// B3PW91LYP/6-311++G(d,p))[a]

structure	ΔG_{vac}	ΔW_0^C	ΔW_0^D	ΔG_{sol}^C	ΔG_{sol}^D
7	0.0	0.0	0.0	0.0	0.0
8	−90.8	61.0	75.6	−29.8	−15.2
9	−85.1	52.8	52.0	−32.3	−33.1
10	−92.2	46.4	51.6	−45.8	−40.6
11	−81.0	44.7	49.8	−36.3	−31.2
12	−123.0	47.2	49.0	−75.8	−74.0
13/2	−156.7	48.1	50.2	−108.6	−106.5
14/2	−151.4	51.0	51.8	−100.4	−99.6
15	−172.6	−17.2	−14.1	−155.4	−158.5
16/2	−126.7	47.7	52.4	−79.0	−74.3
17/2	−139.5	51.1	53.2	−88.4	−86.3
18/2	−151.8	56.3	58.8	−95.5	−93.0
19	0.0	0.0	0.0	0.0	0.0
21	−72.4	27.2	27.6	−45.2	−44.8
24	−61.4	26.7	27.2	−34.7	−34.2
25	−102.3	29.0	33.8	−73.3	−68.5

[a] With respect to the structure **7**, $W_0^D = -64.9$ kcal/mol, $W_0^C = -65.4$ kcal/mol; with respect to the structure **19**, $W_0^D = -45.1$ kcal/mol, $W_0^C = -46.9$ kcal/mol.

with *n*, that is, the EA considerably decreases about 20 kcal/mol from $Li^+(EC)$ to $Li^+(EC)_2$, and then gently decreases. Furthermore, for the given supermolecules, the energy level differences between the two kinds of low virtual orbitals increase also with *n*. For example, it is only −0.007 au for $Li^+(EC)$ (the LUMO occupied by Li^+), whereas it is 0.018 au for $Li^+(EC)_2$, 0.023 au for $Li^+(EC)_3$ and 0.021 au for $Li^+(EC)_4$ (the LUMO occupied by EC). Consequently, the EA difference between the two types of intermediates is sharper for $Li^+(EC)$ than for $Li^+(EC)_2$ (11.1 vs 2.7 kcal/mol). It is predicted that the reduction intermediate corresponding to Li^+ reduction would be much more unstable than that arising from EC reduction.

Compared with the case of $Li^+(EC)_2$, regarding to the radical termination reactions the Gibbs free energies of reaction for path **A** (**37** → **42**, see Figure 4), path **B** (**37** → **39**) and path **C** (**37** → **38**) of $Li^+(EC)_3$ are only slightly decreased by 1.4, 1.6, and 1.0 kcal/mol, respectively. Therefore, path **A** again is the most favorable, and paths **B** and **C** are as competitive as in the case of $Li^+(EC)_2$. As to the secondary reactions of the unpaired lithium carbonate **38** with the supermolecule, $Li^+(EC)_3$, path **F**, resulting in lithium ethylene dicarbonate (**39**, in Figure 4), becomes thermodynamically much more favorable than path **G** that yields lithium carbonate **40** (ΔG, −91.0 vs −81.8 kcal/mol).

Bulk Solvent Effect from Polarized Continuum Models for $Li^+(EC)_n$ ($n = 1-2$). Insights about bulk solvent effects are provided from the C-PCM and D-PCM calculations for the $Li^+(EC)_n$ ($n = 1,2$) models (see Table 7). In the case of Li^+-(EC), all of the ΔG_{sol} from the two methods agree well within 5 kcal/mol, except for the intermediate 8, for which D-PCM predicts destabilization ($W_0 = 10.7$ kcal/mol) in solution, whereas C-PCM gives an opposite effect ($W_0 = -4.4$ kcal/mol). The following discussion will be focused on the C-PCM results. $Li^+(EC)$ and the unpaired lithium carbonate $[Li(CO_3)]^-$ are much more stabilized ($W_0 = -65.4$ and −82.6 kcal/mol, respectively) than the other species through the bulk solvent. Thus, both the adiabatic EA of $Li^+(EC)$ and the free energy release are considerably decreased by roughly one time. The variation trend is qualitatively consistent with that predicted by $Li^+(EC)_n$ ($n = 2-4$). As shown in Table 7, the $Li^+(EC)_2$-PCM calculations predict that the reduction potential (ΔG_{sol}^D) is −44.8 kcal/mol, which is 4.2 kcal/mol higher negative than that obtained from $Li^+(EC)$-PCM (−40.6 kcal/mol). Coupled with the considerable decrease (∼20.0 kcal/mol) of EA by one more explicit solvent molecule, we could thus conclude that a cluster-continuum model is necessary, including both specific and bulk solvent effects, at least for the predictions of EA or reduction potentials. Additionally, in line with the results of $Li^+(EC)_n$ ($n = 2-4$), the free energy barrier in solution for the ring opening of the EC-reduction intermediate **10** is very close to that in the gas phase ($\Delta G_{sol}^{\ddagger} = 12.5 \approx \Delta G_{vac}^{\ddagger} = 11.2$ kcal/mol), which shows that effect of bulk solvent on free energy barrier is very weak.

Concerning the termination reactions of the radical anion, again consistent with the trend from the more complex model calculations, the ΔG_{sol} for paths **A**, **B**, and **E** become slightly less negative as compared with those of $Li^+(EC)$. In addition, the numerical data for the continuum and the explicit solvent model are similar: ΔG_{sol} for paths **A**, **B**, and **E**, −65.6, −49.2, and −55.2 kcal/mol versus $\Delta G_{vac} = -65.4$, −49.0 kcal/mol for **A** and **B** from $Li^+(EC)_3$ and −58.4 kcal/mol for path **E** from $Li^+(EC)_2$. The ΔG_{sol} for path **D** becomes more negative than that predicted for $Li^+(EC)_2$ ($\Delta G_{sol} = -52.4$ kcal/mol vs $\Delta G_{vac} = -37.9$ by $Li^+(EC)_2$). Although the absolute data of ΔG_{sol} for paths **F** and **G** are also much different than those of the $Li^+(EC)_3$ model, it is demonstrated that path **F** becomes more favorable at high EC concentration ($\Delta G_{sol} = -45.4$ vs −35.6 kcal/mol). Due to shortage of data regarding the solvation energy of an electron, the ΔG_{sol} of path **C** is not addressed.

Comparison with Experimental Reduction Potentials of EC-Based Solvents. To quantitatively discuss the lithium reduction potential in EC-based nonaqueous electrolyte, a thermodynamic chemical cycle for the lithium electrode reaction is applied.[48]

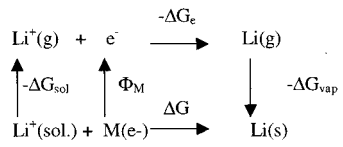

$$\Delta G = -\Delta G_{sol} + \Phi_M - \Delta G_e - \Delta G_{vap}$$
$$= G(Li^+,g) - G(Li^+,sol.) + \Phi_M + G(Li,g) - G(Li^+,g) - \Delta G_{vap}$$
$$= G(Li,g) - G(Li^+,sol.) + \Phi_M - \Delta G_{vap} \quad (5)$$

where ΔG_{sol} is the solvation free energy of Li^+, Φ_M is the work function of the inert metal electrodes, ΔG_e is the ionization free energy, and ΔG_{vap} is the vaporization free energy. On the basis of eq 5, the difference of the lithium electrode potential between aqueous and organic electrolytes depends only on the variation of free energy of Li^+ in solution, $G(Li^+,sol)$. Because of the rather close dielectric constants (water/78.3 vs EC/89.8), the calculated $G(Li^+,sol)$ in EC solvent is negligibly lower (less than 0.01 eV) than that in aqueous medium (−7.446348 vs −7.446085 au by C-PCM-B3PW91/6-311++G(d,p). Therefore, the lithium electrode potential in EC-based electrolyte should be quite similar to that in aqueous electrolyte, that is, −3.05 V versus SHE (standard hydrogen electrode), −1.5 eV on the physical scale. Additionally, White et al. also stood their discussion on −3.045V of Li^+/Li as dealing with capacity fade in lithium-ion batteries.[12]

(47) Hehre, W. J.; Radom, L.; Schleyer, P. v. R.; Pople, J. A. *Ab Initio Molecular Orbital Theory*; John Wiley & Sons: New York, 1986.

(48) Parker, V. D. *J. Am. Chem. Soc.* **1976**, *98*, 98.

Table 8. Comparisons of the Gibbs Free Energies of Reaction for the Involved Processes (A, B, C, D, E, F, and G) for $Li^+(EC)_n$ ($n = 1-4$)[a]

	A	B	C	D	E	F	G
$Li^+(EC)$	−67.4	−56.8 (−58.7)	−49.2 (−36.8)	−39.6 (−39.8)	−63.8	−130.1 (−138.1)	−131.1 (−142.3)
$Li^+(EC)_2$	−64.0 (−67.6)	−47.4 (−48.6)	−48.5 (−38.2)	−37.9 (−41.0)	−58.4 (−63.0)	−101.1 (−107.4)	−97.0 (−107.4)
$Li^+(EC)_3$	−65.4 (−72.0)	−49.0 (−52.2)	−49.7 (−42.6)			−91.0 (−95.2)	−81.8 (−88.0)
$Li^+(EC)_4$			−51.7 (−42.5)				

[a] The data in parentheses refer to B3PW91/6-31G(d), others to B3PW91/6-311++G(d,p)//B3PW91/ 6-31G(d).

A lot of experimental efforts have been devoted to investigate the SEI film problem in lithium-ion batteries, using either a lithium anode[15] or a carbon-based insertion anode.[11,49−51] When a carbon electrode is polarized to low potentials in polar aprotic Li salt solutions, electrolyte species will be reduced at potentials higher than that of the Li/Li^+ couple. Naji et al.[11] and Novak et al.[49] separately found that EC is reduced at potentials about 0.8 V versus Li^+/Li (on the physical scale, −2.36 eV), and Yamaguchi et al. reported that at a potential of approximately 1.0 V versus Li^+/Li (on the physical scale, −2.56 eV) a film begins to form quickly on the anode surface (1:1 EC/EMC, 1 M $LiClO_4$), which could also be ascribed to the EC reduction. The calculated reduction potentials (−EA) from the supermolecule/cluster $Li^+(EC)$-CPCM approach, −45.8 kcal/mol, or −2.0 eV on the physical scale, agree well with these experimental findings. The consistency confirms that a supermolecule/continuum model is necessary to include both specific and bulk solvent effects. The reduction potential is overestimated by the $Li^+(EC)_n$ ($n = 1$, 2) models (ΔG: −92.2, −70.6 kcal/mol, −4.0 and −3.1 eV on the physical scale) because these models account only partially for the solvent effect. The reduction potentials from $Li^+(EC)_3$ and $Li^+(EC)_4$ (ΔG: −61.6,−51.4 kcal/mol, −2.7 and −2.2 eV) become less negative, as found also applying the PCM model to $Li^+(EC)$ and $Li^+(EC)_2$; these values are also similar to the experimental results.

In conclusion for the reduction mechanism, the EC molecule reductive decomposition first encounters an ion-pair intermediate after accepting the electron transferred from the anode. It is this intermediate that determines the further reaction. For the isolated EC molecule, the intermediate is not stable in gas phase, that is, the adiabatic EA of EC is negative. However, a stable intermediate with about 10 kcal/mol lower energy is obtained in EC bulk solvent with the SCIPCM method, and hence the reduction of EC becomes plausible. In the presence of Li^+, EC becomes much more easily reduced than the isolated EC molecule as denoted by its high positive adiabatic EA. The adiabatic EAs decrease with an increasing number of coordinated EC molecules, 20 kcal/mol with the second EC, about 10 cal/mol with each additional EC. This indicates that the reduction of EC is easier at low EC than at high EC concentration. However, the adiabatic EA of $Li^+(EC)_4$ is still quite high, 59.0 kcal/mol. Hence, it may be safe to conclude that the lithium-ion coordinated EC molecule will be initially reduced by the electron transferred from the anode instead of the free EC molecule. Homolytic ring opening will take place in the intermediate via a barrier of about 11.0 kcal/mol, which nearly remains the same independently of the number of EC molecules. The energy release upon radical-anion formation decreases when the EC concentration increases.

Five possible termination ways of the radical anion have been located. Two of them are the barrierless dimerization of radical anion (paths **A** and **B**), bringing about two lithium alkyl dicarbonates, $(CH_2CH_2OCO_2Li)_2$ and $(CH_2OCO_2Li)_2$. This is consistent with the conclusion from Aurbach et al.,[46] Naji et al.,[11] and Bar-Tow et al.[17] The third one is a further reduction by the second electron transferred from the polarized electrode (path **C**), by which a weak complex of ethylene gas and an unpaired nucleophilic carbonate anion ($LiCO_3^-$) are generated. Another possible path is the formation of a solvated species containing C−Li bonds (Li carbides), $Li(CH_2)_2OCO_2Li$. This product is formed via electron pairing between the radical anion and the reduction intermediate in which Li^+ is reduced (path **D**), as it has been detected with the XPS technique.[15,17] The reaction of the radical anion with another subproduct of EC reduction is also possible (path **E**), resulting in a compound containing an O−Li bond and an ester group. In terms of the ratio of required electrons per consumed EC molecule, paths **A**, **B**, and **E** could be classified as one-electron reduction processes, paths **C** and **D** as two-electron processes.

From Table 8, the Gibbs free energies of reaction for paths **A**, **C**, and **D** are not sensitive to the number of EC molecules in $Li^+(EC)_n$ ($n = 1$, 2, and 3), whereas for path **B**, ΔG increases by 9.4 kcal/mol from $Li^+(EC)$ to $Li^+(EC)_2$, but from $Li^+(EC)_2$ to $Li^+(EC)_3$ it shows a small decrease of 1.6 kcal/mol. The paths **F** and **G**, starting from $(LiCO_3)^-$ have very similar ΔG in the case of $Li^+(EC)$, whereas **F** becomes more and more favorable for the cases of $Li^+(EC)_2$ and $Li^+(EC)_3$. This shows that a weak EC concentration dependence of the SEI components exists. These results indicate that lithium alkyl dicarbonates $(CH_2OCO_2Li)_2$ (from paths **F** and **B**), $(CH_2CH_2OCO_2Li)_2$ (path **A**) and LiO−R (path **E**) are the major electroreduction products; however, the inorganic product, Li_2CO_3, and C−Li carbide product are indeed generated, especially at low EC concentration. By taking into account the high solubility of lithium butylene dicarbonate and the O−Li bond compound in organic solvent, their contributions to the SEI film may be weak. The whole reaction is shown in Scheme 1.

Conclusions

High-level density functional calculations have been carried out for an isolated EC, and supermolecules such as $Li^+(EC)_n$ ($n = 1-5$) to investigate the reductive decomposition mechanism of EC in electrolyte solutions used in lithium ion batteries. In gas phase, EC is unlikely to be reduced because of its negative adiabatic EA, whereas the effect of a continuum solvent indicates that it could undergo one-electron as well as possibly two-electron reduction processes in solution. The coordination with Li^+ considerably enhances the reduction of EC; however, the adiabatic EAs of $Li^+(EC)$ ($n = 1-4$) decrease with the number of EC molecules independently of EC or Li^+ being reduced. Regarding the reduction mechanism, an EC molecule coordinated with Li^+ is initially reduced to an ion-pair intermediate. The intermediate will undergo homolytic C−O bond cleavage via a barrier of about 11.0 kcal/mol, with the help of an excess electron. This barrier nearly remains the same for $Li^+(EC)_n$. Five possible termination ways of the radical anion coordinated with Li^+ have been investigated. According to a conventional classification, three of them are one-electron

(49) Novak, P.; Joho, F.; Imhof, R.; Panitz, J.-C.; Haas, O. *J. Power Sources* **1999**, *81−82*, 212.
(50) Imhof, R.; Novak, P. *J. Electrochem. Soc.* **1998**, *145*, 1081.
(51) Yamaguchi, S.; Asahina, H.; Hirasawa, K. A.; Sato, T.; Mori, S. *Mol. Cryst. Liq. Cryst.* **1998**, *322*, 239.

Scheme 1. EC/Li^+ Reductive Decomposition Mechanism

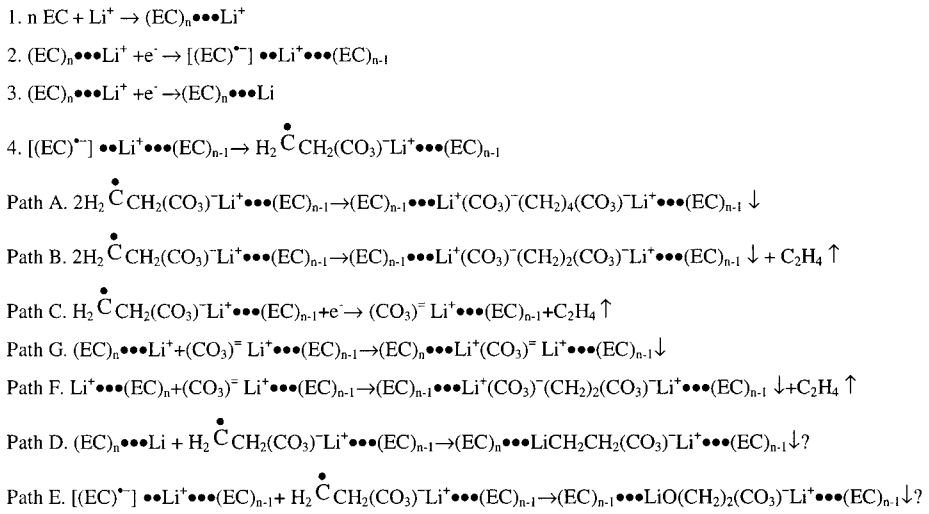

reduction processes and result in lithium ethylene dicarbonate, $(CH_2OCO_2Li)_2$ + ethylene (path **B**), lithium butylene dicarbonate $(CH_2CH_2OCO_2Li)_2$ (path **A**), and an O−Li compound with an ester group, $LiO(CH_2)_2CO_2(CH_2)_2OCO_2Li$ (path **E**), respectively, while two of them could be interpreted as two-electron reduction processes, generating a weak complex of an unpaired nucleophilic carbonate anion ($LiCO_3^-$) with ethylene gas (path **C**) and a C−Li bond compound (Li carbide), $Li(CH_2)_2OCO_2Li$ (path **D**). Thermodynamically, the most favorable is path **A**, followed by path **E**, then by two very competitive paths **C** and **B**, and finally by the least favorable path **D**. Further reactions of $LiCO_3^-$ with the supermolecule only exhibits a weak EC concentration preference for the generation of $(CH_2OCO_2Li)_2$ (path **F**) to Li_2CO_3 (path **G**).

On the basis of the results presented here, it may be inferred that surface films resulting from solvent reduction comprise $(CH_2CH_2OCO_2Li)_2$, $(CH_2OCO_2Li)_2$, $LiO(CH_2)_2CO_2(CH_2)_2OCO_2Li$, $Li(CH_2)_2OCO_2Li$, and Li_2CO_3. $(CH_2OCO_2Li)_2$ could be generated by path **B** as well as path **F**, whereas inorganic Li_2CO_3 only by path **G**. Taking into account the higher solubilities of $(CH_2CH_2OCO_2Li)_2$ and $LiO(CH_2)_2CO_2(CH_2)_2OCO_2Li$, as compared with $(CH_2OCO_2Li)_2$, their contribution to the SEI film would be weak, but the more negative ΔG of their formation paths (**A** and **E**) compared to that of the formation path (**B**) of $(CH_2OCO_2Li)_2$ to some extent compensates for the loss. Regarding the composition of the surface films resulting from solvent reduction, for which experiments usually indicate that $(CH_2OCO_2Li)_2$ is a dominant component, we therefore conclude that they are comprised by two leading lithium alkyl bicarbonates, $(CH_2CH_2OCO_2Li)_2$ and $(CH_2OCO_2Li)_2$, together with $LiO(CH_2)_2CO_2(CH_2)_2OCO_2Li$, $Li(CH_2)_2OCO_2Li$ and Li_2CO_3.

Acknowledgment. This work was partially supported by NSF (Career Award Grant CTS-9876065 to P.B.B.), by Mitsubishi Chemical Corporation, and by DOE Cooperative Agreement DE-FC02-91ER75666. We acknowledge supercomputer resources provided by the National Computational Science Alliance under Grants CHE000040N, CTS000016N, CTS00007N (Y.W., P.B.B.) and by the National Energy Research Scientific Computing Center, NERSC.

Supporting Information Available: Table S1 tabulates the energy levels and main components for the two lower virtual orbitals for $Li^+(EC)_n$ ($n = 1-4$) corresponding to Li^+ and EC reduction, respectively. Table S2 lists the absolute energies of all the involved stationary points, their structures are collected in Table S3 in Gaussian archive format (PDF). This material is available free of charge via the Internet at http://pubs.acs.org.

JA0164529